Journal of Geophysical Research: Biogeosciences

Supporting Information for

Dry season greening and water stress in Amazonia: the role of modeling leaf phenology

Gabriele Manoli[1], Valeriy Y. Ivanov[2], Simone Fatichi[1]

[1]Institute of Environmental Engineering, ETH Zurich, Zurich, Switzerland

[2]Department of Civil and Environmental Engineering, University of Michigan, Ann Arbor, MI, USA

Contents of this file

Introduction

Simulations were carried out using the mechanistic ecohydrological/biosphere model T&C [Fatichi, 2010; Fatichi et al., 2012a,b]. Model equations for photosynthesis and transpiration are presented in Text S1. Supplementary model results are presented in Fig. S1-S12. Calibrated model parameters are listed in Table S1. Model results are discussed in Text S2. References are listed in the main text.

Text S1.

Photosynthesis is simulated in T&C using recent modifications of the Farquhar biochemical model [Farquhar et al., 1980; Bonan et al., 2011]. A "two big leaves" scheme, whit sunlit and shaded leaves treated separately, is used to compute net assimilation and stomatal conductance. Stomatal conductance is modeled according to Leuning, (1995):

$$g_s = g_0 + a_1 \frac{A_n}{C_i - \Gamma^*} f(VPD) P_{atm}, \quad (1)$$

where a_1 [-] is an empirical parameter, g_s [μmol CO2 m^{-2} s^{-1}] is the stomatal conductance to CO2, A_n [μmol CO2 m^{-2} s^{-1}] is the net assimilation rate, C_i is the leaf interior partial CO2 pressure, Γ^* [Pa] is the CO2 compensation point, VPD [Pa] is the vapor pressure deficit, P_{atm} [Pa] is the atmospheric pressure, g_0 [μmol CO2 m^{-2} s^{-1}] is the cuticular conductance when $A_n \leq 0$, and $f(VPD)$ is the function of sensitivity to vapor pressure deficit. The net assimilation rate at the leaf scale is given by:

$$A_n = \beta_s(\Psi_L) A^* - R_d, \quad (2)$$

where β_s [-] is a sigmoidal water stress factor, Ψ_L [MPa] is the leaf water potential, A^* [μmol CO2 m^{-2} s^{-1}] is the gross assimilation rate and R_d [μmol CO2 m^{-2} s^{-1}] is the leaf maintenance respiration. Note that $A^* = A^*(C_i, V_{c,max25}, e_{rel}, \dots)$ is described by a biochemical model of photosynthesis [Farquhar et al., 1980] and is obtained by solving two quadratic equations [Collatz et al., 1991]. Hence, g_s and A_n are directly impacted by the relative photosynthetic capacity e_{rel} via A^*. Photosynthesis is upscaled from the leaf to the canopy scale assuming an exponential profile of leaf nitrogen content per unit of area and scaling factors for the photosynthetic capacity of the sunlit and the shaded fractions ($F_{sun}$and F_{shade}, respectively) of the leaf area index LAI [Mastrotheodoros et al., 2017]. Also, note that daily gross primary production is defined as $GPP = k(\mathrm{A}_n + R_d)$ [gC m^{-2} s^{-1}], where k is a unit conversion factor.

Transpiration fluxes are estimated for sunlit and shaded leaves computing the specific humidity at saturation q_{sat} [-] at the corresponding surface temperature T_s [°C]. For instance, transpiration from sunlit leaves is defined as:

$$T = \frac{\rho_a [q_{sat}(T_s) - q_a]}{r_a + \frac{r_b}{LAI \cdot F_{sun}} + \frac{r_{s,sun}}{LAI \cdot F_{sun}}}, \quad (3)$$

where ρ_a is the air density, q_a is the specific humidity, r_a [s m^{-1}] is the aerodynamic resistance to vapor flux, r_b [s m^{-1}] is leaf boundary layer resistance, and $r_{s,sun} = 1/g_{s,sun}$ [s m^{-1}] is the stomatal resistance of sunlit leaves. We refer to [Fatichi, 2010; Fatichi et al., 2012a,b] for a detailed description of model formulation and parameters.

Text S2.

An illustrative example of the variables affected by the tropical phenology module developed for tropical rainforests is illustrated in Fig. S1. Simulation results are shown for a given year at site km34.

The location of the study sites as well as the soil properties from the SoilGrids250m database by ISRIC World Soil Information [Hengl et al., 2017] are illustrated in Figure S2. Calibrated model parameters for both T&C model versions (i.e. with and without tropical phenology) are listed in Table S1.

Additional model results are provided in Figures S3-S12. A comparison of simulated and observed surface energy fluxes (net radiation, sensible and latent heat) at sites km67 and km34 are presented in Figures S3, S5 for the original T&C formulation and in Figures S4, S6 for T&C with tropical phenology. The inclusion of a leaf-phenology model clearly improves GPP seasonal dynamics while preserving a good agreement between observed and simulated energy fluxes. A comparison of simulated and observed soil moisture dynamics is also presented in Fig. S7.

To elucidate the mechanisms generating the patterns observed in Fig. 6 and 7 (main text) we present here simulation results for site km67 and Vilafranca obtained by the original and modified (i.e. with leaf phenology) T&C model versions. Figures S8-S9 show a comparison of carbon assimilation A_n, leaf internal CO2 concentration C_i, stomatal conductance g_s (per unit leaf), leaf area index (LAI), total canopy conductance g_c (per unit ground) and evapotranspiration (ET). Note that leaf phenology generally decreases A_n and g_s, with little impact on C_i. However, changes in ET (and g_c) are limited (Fig. S9c,f). From Equations 2 and 3, it is clear that the impact of leaf phenology (encoded in e_{rel}) directly affects A_n and g_s but is buffered by leaf-atmosphere decoupling [De Kauwe et al., 2017] and LAI variations (i.e. the series of resistances at the denominator of Eq. 3) which act to limit the changes ΔET when compared to ΔA_n (Fig. S8-S9). Figures S10-S11 show the same variables illustrated in Fig. S8-S9 but simulations with and without phenology are run using the same set of model parameters (calibrated with the phenology module on). These results confirm that, compared to the introduction of phenology, model calibration has little impact on the observed changes in carbon and water fluxes.

Simulated ET and GPP at the study sites are also compared with empirical observations (remote sensing and upscaled flux tower data) and Dynamics Global Vegetation Model (DGVM) simulations for the entire Amazon basin [Ahlström et al., 2017]. The results (Fig. S12) demonstrate that productivity at the study sites is radiation limited as GPP is high and insensitive to differences in mean annual precipitation (MAP), which is generally > 1500 mm yr^{-1}. The fact that simulated ET is higher than observations for MAP<2000 mm yr^{-1} can be explained by uncertainties in the estimation of observed ET due to well-known issues of flux-tower estimates during rainy periods (see main text) as well as discrepancies between simulations and observations in terms of location and study periods.

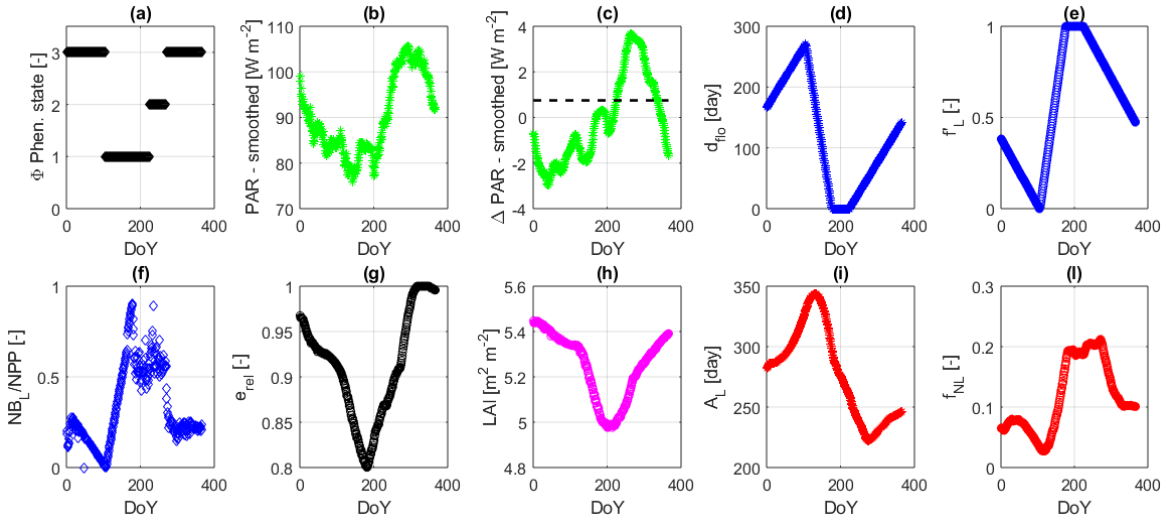

Figure S1. Illustrative example of the variables affected by the tropical phenology module developed for tropical rainforests. A given year from the km34 site is shown (DoY = day of year). (a) φ Phenological state; (b) smoothed PAR; (c) smoothed PAR derivative ($\overline{\Delta \boldsymbol{PAR}}$); (d) phenological index counting days from new season; (e) preliminary allocation fraction to leaves; (f) ratio between new leaf production and NPP, which represent the actual allocation of C to leaves in a given day; (g) relative photosynthetic efficiency; (h) Leaf Area Index; (i) Leaf Age; (l) fraction of new leaves (<1 month) in the total leaf biomass.

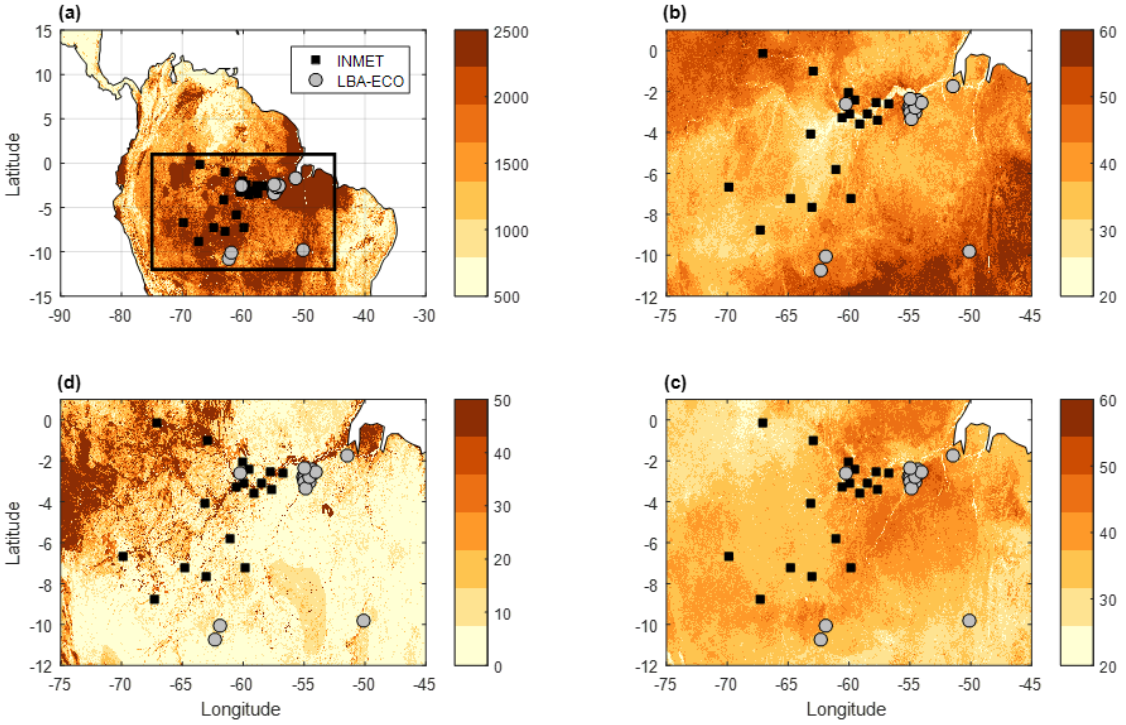

Figure S2. Location of INMET meteorological stations and LBA-ECO flux towers and weather stations (square and circles, respectively). Absolute depth to bedrock [cm] (a), sand content [%] (b), clay content [%] (d) and soil organic carbon content [g kg^{-1}] (c). Data are retrieved from SoilGrids250m database by ISRIC World Soil Information [Hengl et al., 2017]. Data are made available online under the Open Database License (https://soilgrids.org/).

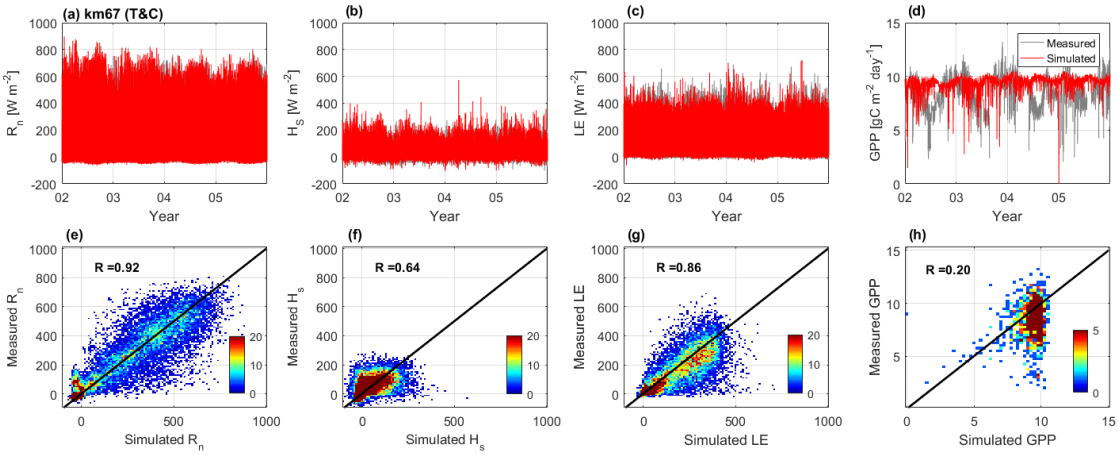

Figure S3. Comparison between measured and simulated net radiation (a,e), sensible heat (b,f), latent heat (c,g) and daily GPP (d,h) at site km67. Simulation results are obtained using the original T&C formulation (i.e. without phenology). Colors indicate the density of observations (points per pixel). The correlation coefficient R is also shown.

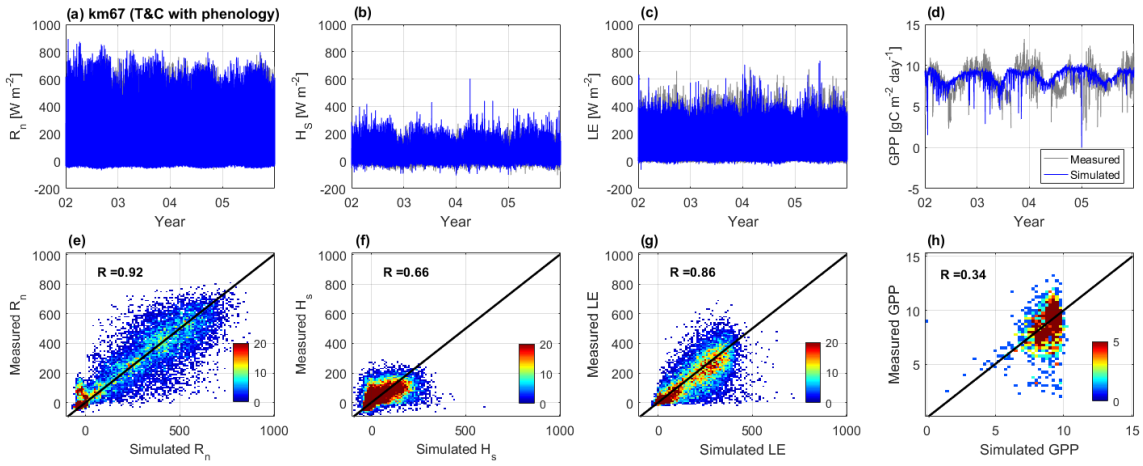

Figure S4. Comparison between measured and simulated net radiation (a,e), sensible heat (b,f), latent heat (c,g) and daily GPP (d,h) at site km67. Simulation results are obtained using the new T&C formulation (i.e. T&C with phenology). Colors indicate the density of observations (points per pixel). The correlation coefficient R is also shown.

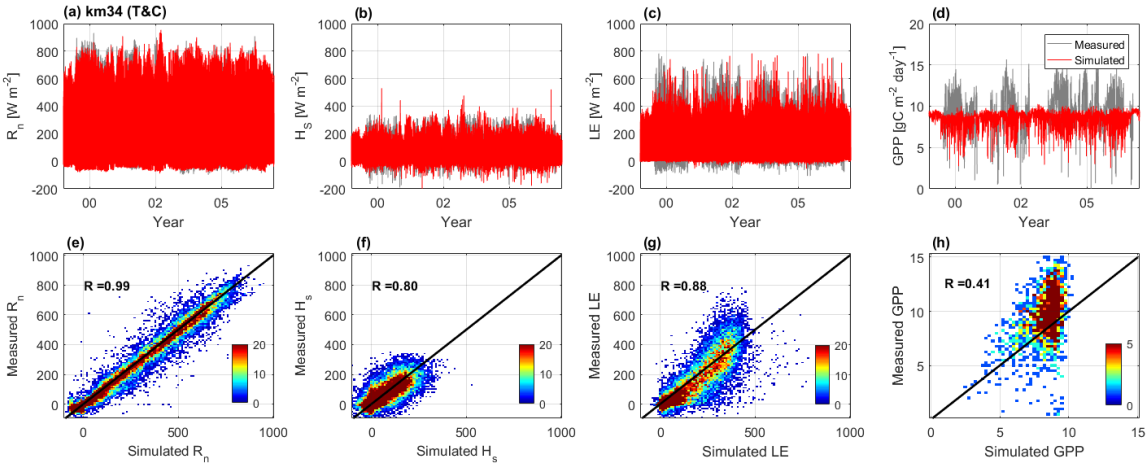

Figure S5. Comparison between measured and simulated net radiation (a,e), sensible heat (b,f), latent heat (c,g) and daily GPP (d,h) at site km34. Simulation results are obtained using the original T&C formulation (i.e. without phenology). Colors indicate the density of observations (points per pixel). The correlation coefficient R is also shown.

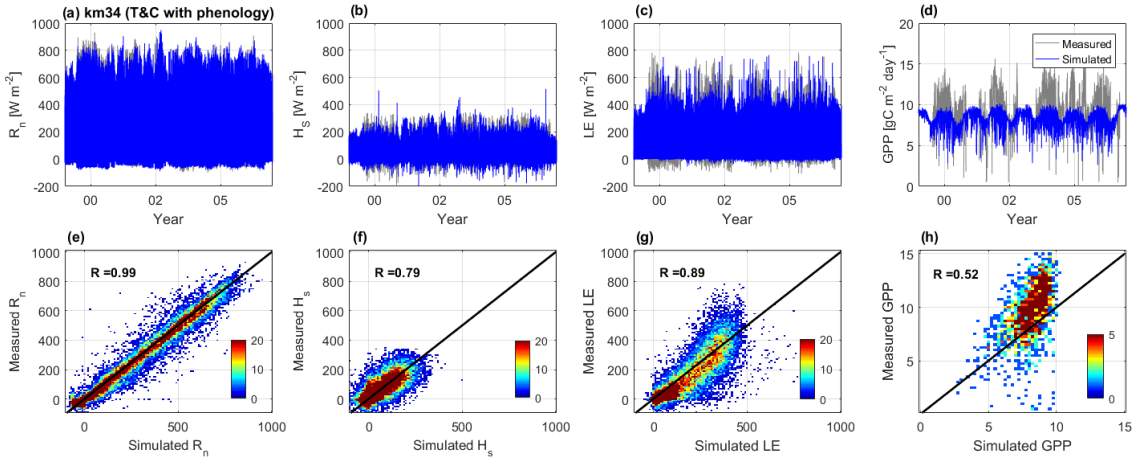

Figure S6. Comparison between measured and simulated net radiation (a,e), sensible heat (b,f), latent heat (c,g) and daily GPP (d,h) at site km34. Simulation results are obtained using the new T&C formulation (i.e. T&C with phenology). Colors indicate the density of observations (points per pixel). The correlation coefficient R is also shown.

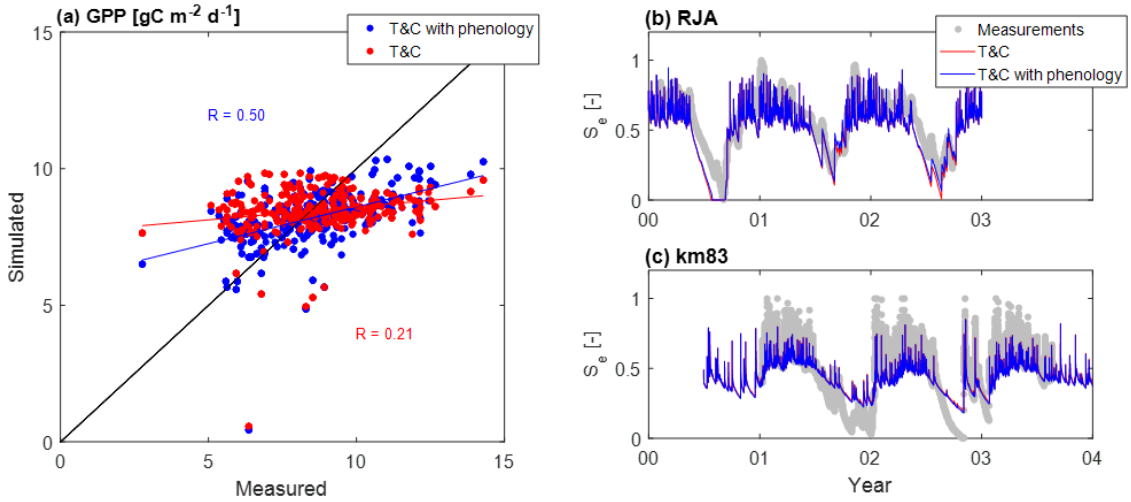

Figure S7. Flux tower measured and simulated GPP, as monthly averages across the different study sites where GPP data are available (a), and effective saturation at 10 cm depth, Se, for sites RJA (b) and km83 (c). In panel (a) the correlation coefficient R is also shown.

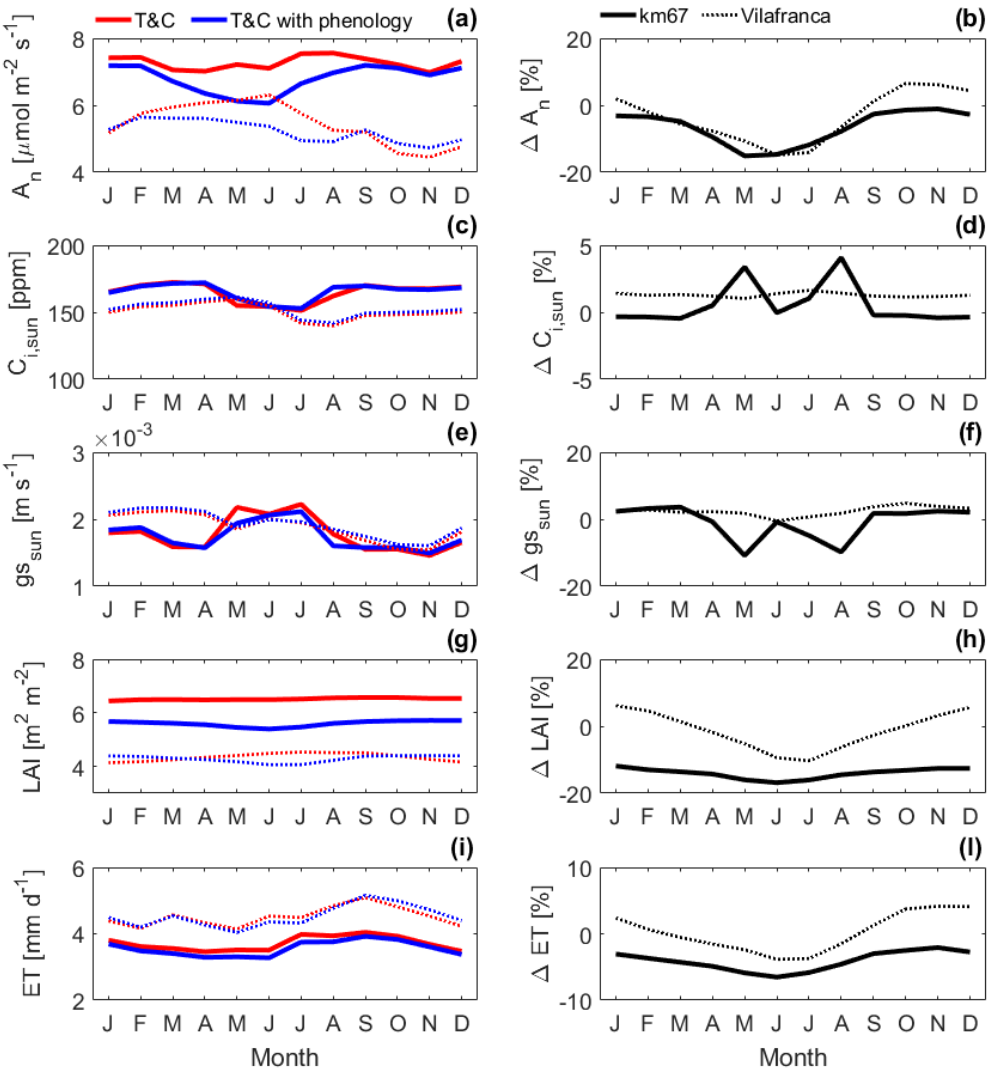

Figure S8. Simulation results by the original (T&C) and modified (T&C with phenology) model versions: (a) carbon assimilation $\boldsymbol{A_n}$ [µmol m^{-2} s^{-1}], (c) internal CO2 concentration of sunlit leavs $\boldsymbol{C_{i,sun}}$ [ppm], (e) stomatal conductance of sunlit leaves during daytime $\boldsymbol{g_{s,sun}}$ [m s^{-1}], (g) LAI [m^2 m^{-2}], and (i) evapotranspiration ET [mm d^{-1}]. Results are shown for km67 (solid lines) and Vilafranca (dashed lines). Phenology-induced changes are shown in panels b, d, f, h, and l.

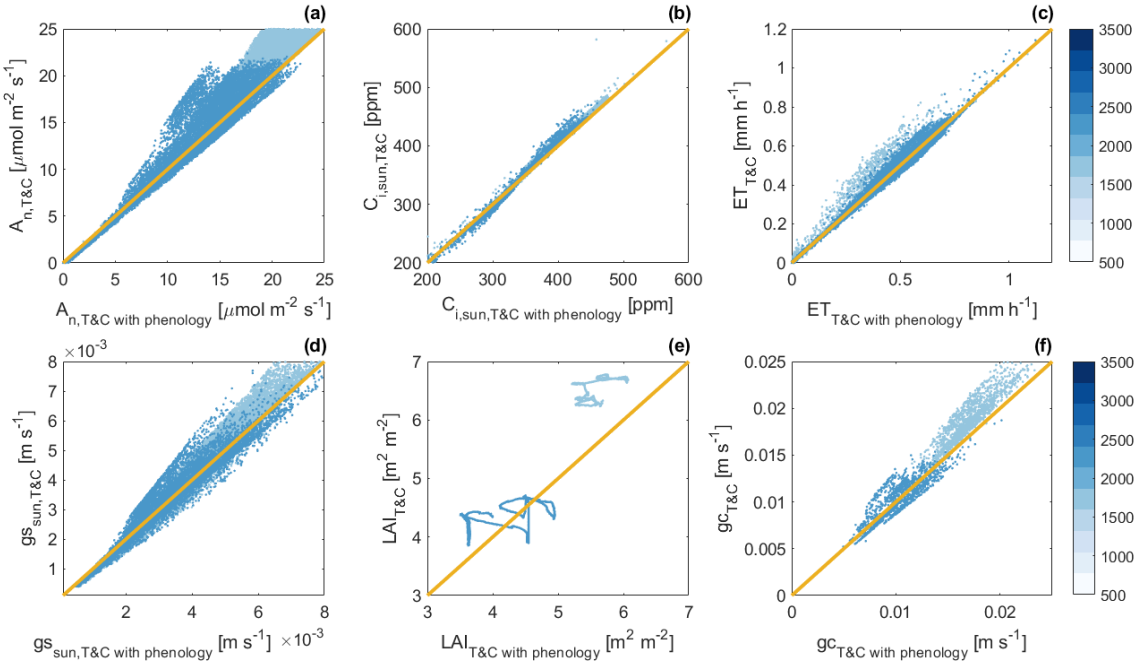

Figure S9. Comparison of simulation results with and without leaf phenology: (a) carbon assimilation $\boldsymbol{A_n}$ [µmol m^{-2} s^{-1}], (b) internal CO2 concentration of sunlit leavs $\boldsymbol{C_{i,sun}}$ [ppm], (c) evapotranspiration ET [mm h^{-1}], (d) stomatal conductance of sunlit leaves during daytime $\boldsymbol{g_{s,sun}}$ [m s^{-1}], (e) LAI [m^2 m^{-2}], and (f) canopy conductance $\boldsymbol{g_c}$ [m s^{-1}]. Simulated hourly (panels a-d) and daily (e-f) values are shown for sites km67 and Vilafranca. Colors indicate MAP [mm yr^{-1}] as in Fig. 6 in the main text. The 1:1 line is also illustrated for comparison (yellow line).

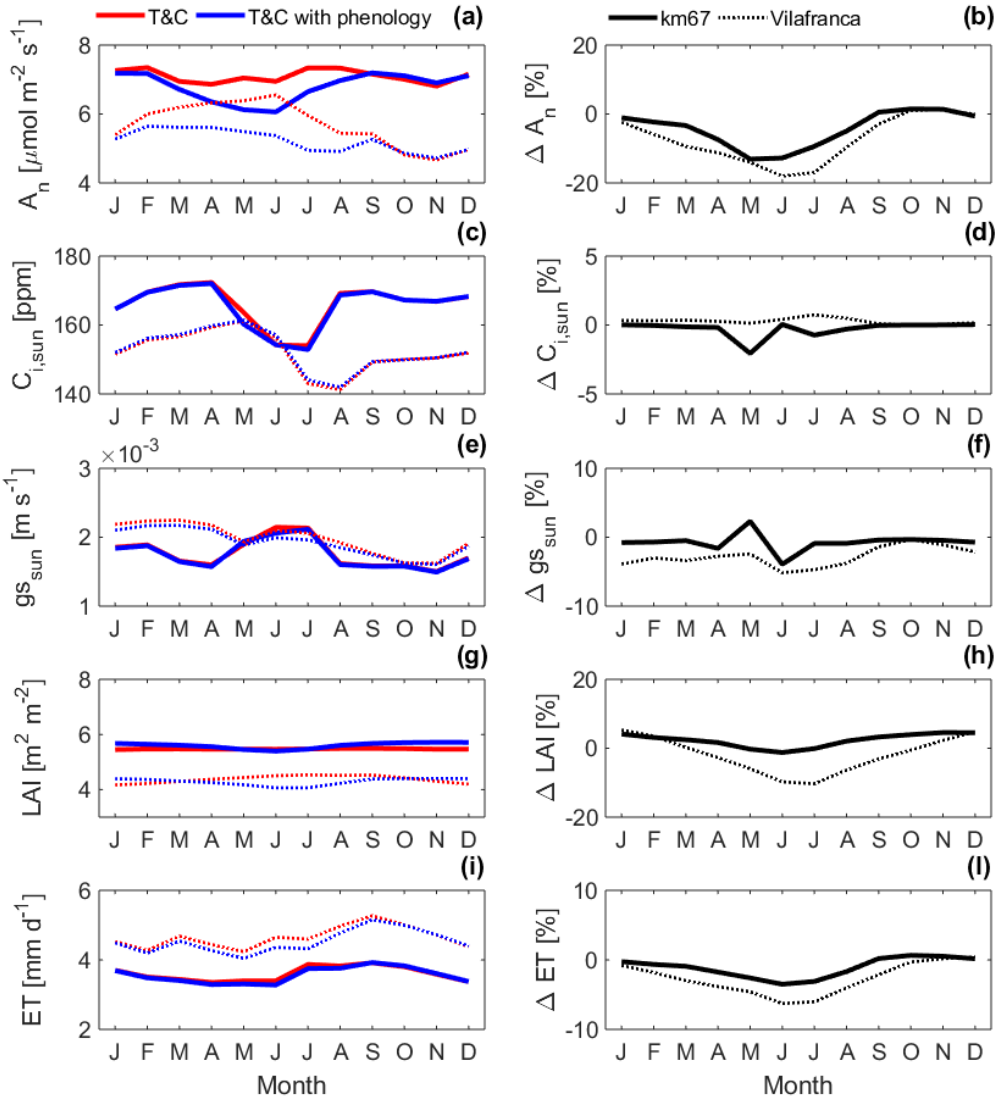

Figure S10. Same as Fig. S8 but simulations with and without phenology are run using the same set of model parameters (calibrated considering phenology).

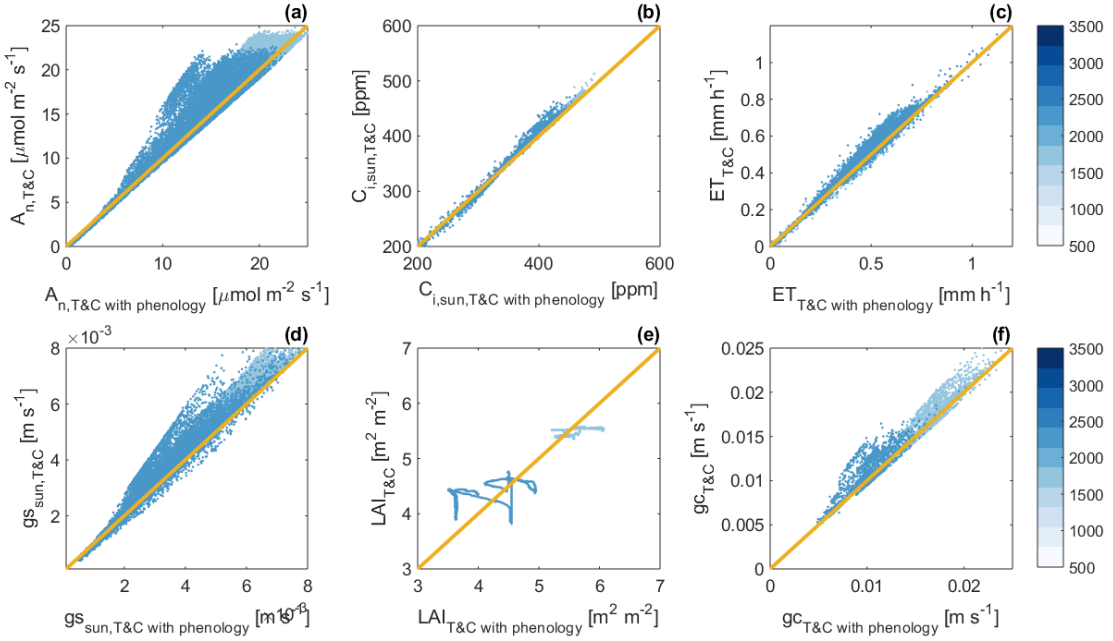

Figure S11. Same as Fig. S9 but simulations with and without phenology are run using the same set of model parameters (calibrated considering phenology).

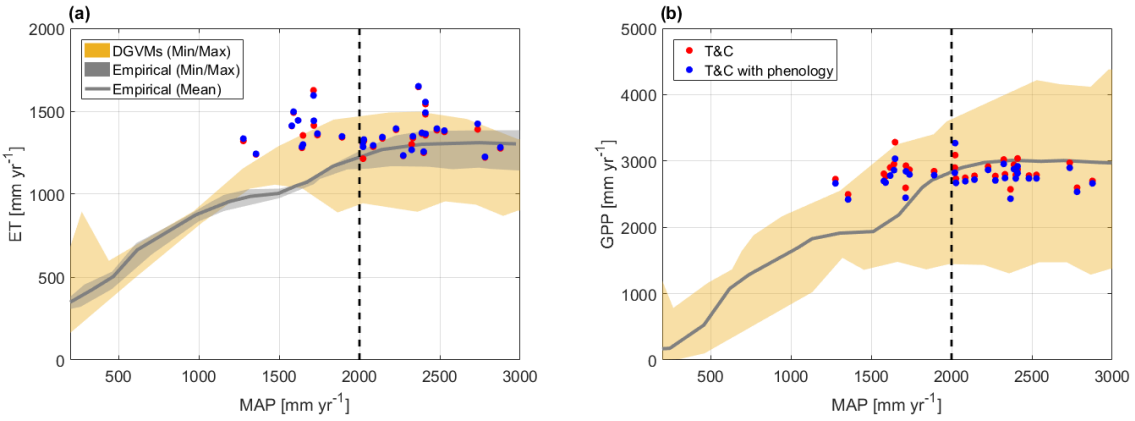

Figure S12. Simulated changes in ET (a) and GPP (b) as a function of mean annual precipitation (MAP) compared with empirical observations (remote sensing and flux tower data) and DGVM simulations by Ahlstrom et al. [Ahlström et al., 2017]. The dashed black line indicates the breakpoint between what are assumed to be water-limited (MAP ≤ 2000 mm yr^{-1}) and radiation-limited (MAP>2000 mm yr^{-1}) conditions [Guan et al., 2015; Ahlström et al., 2017].

		T&C						T&C with phenology					
Parameter	**Unit**	**km34**	**km67**	**km83**	**CAX**	**RJA**	**Avg.**	**km34**	**km67**	**km83**	**CAX**	**RJA**	**Avg.**
ZR95	m	10	10	10	3	3	7.2	10	10	10	3	3	7.2
h_c	m	35	35	35	32.5	30	35	35	35	35	32.5	30	35
a_1	-	6	8	7	6	7	6.8	7	8	8	7	7	7.4
ψ_{G50}	MPa	-1.3	-1.3	-1.3	-1.3	-1.3	-1.3	-1.3	-1.7	-1.7	-1.3	-1.7	-1.54
Ψ_{S2}	MPa	-0.9	-0.9	-0.9	-0.9	-0.9	-0.9	-0.9	-0.9	-0.9	-0.9	-0.9	-0.9
Ψ_{S50}	MPa	-1.7	-1.7	-1.7	-1.7	-1.7	-1.7	-1.7	-1.7	-1.7	-1.7	-1.7	-1.7
S_L	-	0.017	0.018	0.015	0.014	0.016	0.016	0.02	0.019	0.019	0.019	0.019	0.019
r	gC/gN/d	0.072	0.058	0.064	0.07	0.062	0.065	0.072	0.058	0.072	0.072	0.072	0.069
$A_{L,cr}$	d	365	365	365	365	365	365	270	270	270	270	270	270
d_{mg}	d	35	35	35	35	35	35	45	45	45	45	45	45
T_{rr}	gC/m^2/d	1	1	1	1	1	1	0.5	0.5	0.5	0.5	0.5	0.5
L_{tr}	-	1.2	1.3	1.1	1.3	1.3	1.24	1.25	1.25	1.25	1.25	1.25	1.25
ε_{ac}	-	0.15	0.05	0.05	0.05	0.05	0.07	0.15	0.15	0.15	0.15	0.15	0.15
$1/K_{Lf}$	d	40	40	40	40	40	40	15	15	15	15	15	15
$V_{c,max25}$	-	50	50	48	48	48	48.8	49	49	47	52	50	49.4
r_{JV}	-	2.2	2.2	2.2	2.2	2.2	2.2	2.2	2.2	2.2	2.2	2.2	2.2
ΔPAR_{th}	-	-	-	-	-	-	-	0.75	0.75	0.75	0.75	1	0.8

ZR95 = root depth 95 percentile, h_c = canopy height, , a_1 = empirical parameter connecting stomatal aperture and net assimilation, ψ_{G50} = water potential for allocation control, ψ_{S2} = water potential at 2% stomatal closure, ψ_{S50} = water potential at 50% stomatal closure, S_L = specific leaf area, r = respiration rate at 10°C, $A_{L,cr}$ = critical leaf age, d_{mg} = days of maximum growth, $T_{r\,r}$ = translocation rate from carbohydrate reserve, L_{tr} = leaf to root biomass maximum ratio, ε_{ac} = parameter for allocation to carbon reserves, K_{Lf} = dead leaf fall turnover, $V_{c,max25}$ = maximum Rubisco capacity at 25°C leaf level, r_{JV} = scaling J_{max} -$V_{c,max}$, ΔPAR_{th} = threshold for leaf phenology model.

Table S1. Calibrated model parameters for the original (T&C) and new (T&C with phenology) model versions. The resulting sets of average biome-specific parameters are also shown.